International Journal of Nanomedicine

Dovepress
open access to scientific and medical research

Open Access Full Text Article

ORIGINAL RESEARCH

Study on the Antibacterial Activity and Bone Inductivity of Nanosilver/PLGA-Coated TI-CU Implants

Zhaoli Geng[1–3], Renping Dong[3], Xinlin Li[1,2], Xinyi Xu[1,2], Lin Chen[1,2], Xu Han[1,2], Dongxu Liu[1,2], Yi Liu[1,2]

[1]Department of Orthodontics, School and Hospital of Stomatology, Cheeloo College of Medicine, Shandong University, Jinan, Shandong, 250012, People's Republic of China; [2]Shandong Key Laboratory of Oral Tissue Regeneration & Shandong Engineering Research Center of Dental Materials and Oral Tissue Regeneration & Shandong Provincial Clinical Research Center for Oral Diseases, Jinan, Shandong, 250012, People's Republic of China; [3]Department of Stomatology, Qingdao West Coast New Area People's Hospital, Qingdao, Shandong, 266400, People's Republic of China

Correspondence: Yi Liu, Department of Orthodontics, School and Hospital of Stomatology, Cheeloo College of Medicine, Shandong University, No. 44-1 Wenhua Road West, Jinan, Shandong, 250012, People's Republic of China, Tel +86-531-88381630, Email yiliu@sdu.edu.cn

Background: Implants are widely used in the field of orthopedics and dental sciences. Titanium (TI) and its alloys have become the most widely used implant materials, but implant-associated infection remains a common and serious complication after implant surgery. In addition, titanium exhibits biological inertness, which prevents implants and bone tissue from binding strongly and may cause implants to loosen and fall out. Therefore, preventing implant infection and improving their bone induction ability are important goals.

Purpose: To study the antibacterial activity and bone induction ability of titanium–copper alloy implants coated with nanosilver/poly (lactic-co-glycolic acid) (NSPTICU) and provide a new approach for inhibiting implant-associated infection and promoting bone integration.

Methods: We first examined the in vitro osteogenic ability of NSPTICU implants by studying the proliferation and differentiation of MC3T3-E1 cells. Furthermore, the ability of NSPTICU implants to induce osteogenic activity in SD rats was studied by micro-computed tomography (micro-CT), hematoxylin-eosin (HE) staining, masson staining, immunohistochemistry and van gieson (VG) staining. The antibacterial activity of NSPTICU in vitro was studied with gram-positive *Staphylococcus aureus (Sa)* and gram-negative *Escherichia coli (E. coli)* bacteria. *Sa* was used as the test bacterium, and the antibacterial ability of NSPTICU implanted in rats was studied by gross view specimen collection, bacterial colony counting, HE staining and Giemsa staining.

Results: Alizarin red staining, alkaline phosphatase (ALP) staining, quantitative real-time polymerase chain reaction (qRT-PCR) and western blot analysis showed that NSPTICU promoted the osteogenic differentiation of MC3T3-E1 cells. The in vitro antimicrobial results showed that the NSPTICU implants exhibited better antibacterial properties. Animal experiments showed that NSPTICU can inhibit inflammation and promote the repair of bone defects.

Conclusion: NSPTICU has excellent antibacterial and bone induction ability, and has broad application prospects in the treatment of bone defects related to orthopedics and dental sciences.

Keywords: nanosilver/PLGA coating, implant infection, antibacterial, osteogenesis, titanium copper alloy

Introduction

Ti and its alloys are widely used in orthopedic fields due to their superior mechanical properties, biocompatibility and resistance to corrosion.[1–4] However, the stress shielding[5] and bioinertness of titanium implants often leads to poor osseointegration, which eventually results in the failure of the implant.[6–9] In addition, titanium implants lack antibacterial properties.[10,11] Implant-associated infection caused by bacteria such as *Staphylococcus aureus* is a very common complication of orthopedic implants and may lead to pain, inflammation, functional decline and implant loosening, seriously affecting the health and quality of life of patients.[12,13] Approximately 18% of implant failures are reported to be attributable to aseptic loosening due to inadequate osseointegration, while 20% are attributed to bacterial infection, and some are attributed to

Received: 27 January 2024
Accepted: 21 May 2024
Published: 24 June 2024

both.[14,15] Therefore, in order to achieve better clinical results, there is an urgent need to develop implants with both antimicrobial and osteogenic properties.

To produce Ti implants with antimicrobial properties, various strategies, such as coating with hydrophilic and antibacterial biomaterials,[16] depositing silver ions containing multilayered polyelectrolyte films,[17] coupling antibiotics,[18,19] and chemical grafting of polycations[20,21] to a Ti substrate, have been developed. However, the antibacterial properties of the substrates obtained by the above methods are often accompanied by cytotoxic side effects. Therefore, it is necessary to develop new methods to confer antimicrobial properties on the Ti matrix without sacrificing the normal biological function of osteoblasts.[22]

With the development of nanotechnology, silver nanoparticles (AgNPs) have gradually become the focus of bone tissue engineering research; their antibacterial ability has been confirmed in previous studies, and some studies have pointed out that they also have a certain ability to promote bone growth. Cao et al[23] utilized plasma AgNPs prepared by bulk immersion ion implantation and fixed on the surface of titanium. They found that AgNPs can promote the osteogenic differentiation of rat bone marrow stem cells. Zhang et al[24] also demonstrated the bone-promoting effect of AgNPs.

Many studies have demonstrated that 5 to 50nm diameter silver nanoparticles exhibit broad-spectrum antibacterial properties, are biosafe and can be used in clinical medicine.[25,26] However, due to the tendency of silver nanoparticles to aggregate and form large clusters, many polymers have been used to stabilize silver nanoparticles; among them, poly(lactic-co-glycolic acid) (PLGA) is an ideal choice and is widely used in the clinic.[27–30] PLGA has been approved by the United States Food and Drug Administration (FDA) for clinical applications.[31] Our group's previous results showed that a nanosilver/PLGA coating can improve the antibacterial activity and bone inductivity of implants. However, since antibacterial substances are present only on the surface of the material, the antibacterial activity of this coating may gradually decline or be completely lost due to friction loss or degradation during use. Therefore, other methods are needed to enhance the stability of the antibacterial and osteogenic effects of the nanosilver/PLGA coating.

The addition of alloying elements with antibacterial functions to original medical metals is a popular research topic and has great application potential. Copper (Cu) is a recognized antibacterial metal element. It is a common alloying element in metal materials and an essential trace element for the human body. Copper (Cu) and copper ions (Cu^{2+}) are strong antibacterial agents with a wide antibacterial spectrum.[32–34] As an alloy metal, copper is easy to process and can be mixed into various metal materials to enhance its antibacterial properties. For example, several copper-containing stainless steel alloys have been demonstrated to exhibit reliable antibacterial activity against common pathogens.[35,36] Some studies have shown that adding copper to pure titanium is useful for various antibacterial applications.[37–39] The incorporation of Cu leads to the formation of a Cu-rich phase (Ti2Cu phase), which is a key factor leading to the release of Cu^{2+} from Ti-Cu alloys.[40] In addition, copper is a biocompatible element and one of the essential trace elements that maintains human body function. Copper is also involved in enzyme reactions related to bone metabolism. A small amount of copper can regulate the activity of osteoblasts and promote their differentiation. When copper levels are low, bone strength and bone formation are reduced, potentially posing a threat to life. Therefore, increasing attention has been given to the development of copper-containing antibacterial medical metal materials. Chen et al reported that the combination of copper and silver has synergistic antibacterial effects;[41] their synergistic effect has been shown to be effective against drug-resistant bacteria, which may be due to increased cell permeability.[10,42] Other studies have shown that a combination of Cu and Ag not only provides the implant with bactericidal ability but also endows it with osteogenic and osseointegration ability.[43]

In this study, we combined nanosilver particles with an antibacterial titanium–copper alloy to prepare a nanosilver/PLGA-coated titanium–copper alloy implant material with antibacterial and osteogenic properties. We aimed to achieve uniform external and internal surface modifications to meet the requirements of promoting bone integration and antibacterial activity. Notably, this is the first report of AgNPs/PLGA TICU and the first time it has been applied to orthopedic implants. In this study, we evaluated the antibacterial properties of nanosilver/PLGA-coated titanium–copper alloy (NSPTICU) in vitro and in vivo to evaluate its potential as an implant material for orthopedic surgery. In addition, we investigated the in vitro and in vivo osteogenic induction properties of NSPTICU.

Materials and Methods

Pretreatment of the Material Surface

Titanium alloy sheets (TI6AL4V) (Xi'an Baoti Group Co., Ltd., Xi'an, China) (diameter 6.5 mm, thickness 1 mm) and titanium-copper alloy sheets (TI6AL4V-CU) (Chinese Academy of Sciences, China) (diameter 6.5 mm, thickness 1 mm) were polished with 600, 800, 1000, and 1200 mesh silicon carbide water sandpaper to remove the surface of the oxide layer and any pollutants. The preliminarily treated titanium sheet and titanium-copper alloy were placed in acetone, anhydrous ethanol and deionized water[44] and subjected to ultrasonic cleaning for 15 minutes. The material was then thoroughly air-dried on a super clean workbench and stored in a container. The materials were sterilized with an ultraviolet lamp before use. The chemical compositions of the titanium alloy and titanium copper alloy are shown in Table 1.

Preparation of the Nanosilver/PLGA Coating

The coating was prepared by the solvent casting method. A certain amount of 20–30 nm silver nanoparticles (Shanghai Naiou Nanotechnology, Shanghai, China), the mass of which was 2% of the total coating mass, was fully mixed with PLGA (Jinan Dagang Biological Engineering Co., Ltd., China) solution dissolved in chloroform (18%) (Tianjin Guangcheng, China) and then placed in a constant temperature shaker for thorough mixing. The titanium alloy and titanium–copper alloy sheets were immersed in the mixed coating solution for 30seconds and then removed to ensure a uniform coating on each material. Care was taken to avoid producing bubbles when applying the coating. Then, the coating was placed in a fume hood to dry completely[45] and the front and back were disinfected with ultraviolet light. These materials were stored at −20 °C until use. Emission scanning electron microscopy (FE-SEM, Bruker, Germany) was used to observe the surface morphology of each group of materials to determine whether the surface coating was complete and uniform and whether silver nanoparticles were deposited or clustered in the coating, as well as to estimate the thickness of the coating. In addition, EDS was used to detect the distribution of elements in the implant surface coating. The mass percentage of nanosilver in the nanosilver/PLGA coating was roughly calculated.

Contact Angle Experiment

A contact angle tester (Dataphysics-OCA20, Germany) was used to test the contact angle of the four different materials. Five microliters of distilled water were dropped on the surface of each group of samples, and static images of the droplets were taken after 5 s of stabilization. The contact angle (θ) of each sample was calculated using contact angle measurement software. If $\theta < 90°$ indicates that the material is hydrophilic, and the smaller the angle is, the better the hydrophilicity; if $\theta > 90°$, the surface of the material is hydrophobic (N=6).

Studies on in vitro Osteogenesis

Cell Culture

Mouse preosteoblasts (MC3T3-E1) (Wuhan Punosai Life Technology Co., Ltd., China) were cultured in complete medium (5% fetal bovine serum (Biological Industries, Israel) and 1% penicillin/streptomycin (Thermo Scientific HyClone, USA), and the remaining cells were cultured in base medium α-MEM (HyClone, USA) and then placed in a cell incubator at 37 °C and 5% CO_2. The medium was changed every two days. Cell passaging was performed when the cells had reached 80–90% confluence in the Petri dish.

Table 1 Chemical Composition (Wt%) of the Material

Element	Al	V	Cu	Fe	C	N	O	H	Ti
Ti6Al4V	5.88	4.02	0.05	0.13	0.05	0.007	0.16	0.015	Balance
Ti6Al4V-Cu	5.90	4.05	5.56	0.16	0.018	0.001	0.09	0.008	Balance

Cell Viability and Proliferation

The proliferation of MC3T3-E1 cells cultured on different materials was evaluated using a cell counting kit 8 (CCK-8, Biosharp, China). The materials of each group were disinfected by ultraviolet rays before use, and the front and back sides were disinfected for 1 h each. Briefly, MC3T3-E1 cells were cultured at a density of 1×10^4 cells/well on the surface of each group of materials for 3, 5, or 7 days. After the time point was reached, the medium was removed and the cells were washed with PBS. CCK-8 reaction solution was added to each well in the dark, and the cells were incubated for 2 h in the dark. After incubation, 100 μL of the mixture was removed from each well and transferred to 96-well plate with a micropipette and then mixed with an enzyme marker (BMG SPECTROstar Nano2, Germany) for 30s, and a wavelength of 450 nm was used to determine the absorbance value of each group.

The cytotoxicity of the materials to MC3T3-E1 cells was detected by a calcein-AM/PI kit (Solarbio, China). MC3T3-E1 cells were inoculated on the surface of each group of materials at a density of 1×10^4 cells/well. The cells were cocultured with the material for 3, 5 or 7 days. The cells were then incubated with preformulated calcein-AM/PI for 20 minutes according to the kit's instructions and observed under an inverted fluorescence microscope (Leica DMI8, Germany).

Alizarin Red Staining and Quantification

MC3T3-E1 cells were inoculated on the surface of different materials, and the inoculation density was 1×10^4 cells/well. On the second day, the original medium was removed and replaced with osteogenic induction solution (α-minimum essential medium supplemented with 10% FBS, 100 nM dexamethasone (Sigma, USA), 1% penicillin–streptomycin, 50 μg/mL ascorbic acid (Sigma, USA), and 10 mM β-glycerophosphate (Sigma, USA). The osteogenic induction solution was changed every two days, and the cells were cultured continuously for 14 or 21 days. After arriving at the time point, the induction results were observed with an Alizarin red staining kit and photographed. After the photographs were taken, the mineralized nodules were quantitatively analyzed using 10% CPC (Solarbio, China), and the absorbance values of each group at 562 nm were determined (N=6).

Alkaline Phosphatase (ALP) Staining and ALP Activity Assay

MC3T3-E1 cells were inoculated on different coated surfaces at a density of 1×10^4 cells/well, cultured in osteogenic induction medium for 7 or 14 days, and stained with a BCIP/NBT alkaline phosphatase staining kit (Biyuntian, China). Images were captured using a stereomicroscope (Nikon SMZ 745T, Japan). ALP activity was determined using an ALP activity kit (Nanjing Institute of Biological Engineering, China) according to the manufacturer's instructions. The sample size for each group was 6.

qRT–PCR Was Used to Detect the Expression of Osteogenic Genes

MC3T3 was inoculated on the surface of each group at a density of 1×10^4 cells/pore, and osteogenic induction was performed for 7 and 14 days. After reaching the indicated time points, total RNA was first extracted with Triquick reagent (Solarbio, China), after which the genomic DNA was removed with an Evo M-MLV reverse transcription kit (AG, China), and then cDNA was obtained via reverse transcription. The RNA reverse transcription process was performed on ice. Finally, we performed RT–PCR on cDNA using the SYBR Green Pro Taq HS Premix qPCR Kit II (Accurate Biology, China) according to the manufacturer's instructions.[15] Triplicate data were analyzed using the $2^{-\Delta\Delta CT}$ method, and GAPDH was used as the internal reference gene for normalization. The primers used for the amplification of different genes via real-time PCR analysis are shown in Table 2 (N=6).

Western Blot

MC3T3 cells were inoculated on each group of samples in a 6-well plate at a density of 2×10^5 cells/well. After 24 h of culture, the medium was changed to osteogenic induction medium. Seven days after osteogenic induction, the cells were collected, and the protein was extracted from the cell lysate. The protein concentration was detected by a BCA kit (Solarbio, China). The proteins were separated by 8% SDS polyacrylamide gel electrophoresis and transferred to PVDF membranes (Millipore, USA). After blocking with 5% skim milk, the appropriate primary antibodies (ALP, COL I, RUNX2, OCN, GAP) were diluted according to the manufacturer's instructions and incubated at 4°C overnight. The next day, the membranes were washed with TBST solution, and incubated with secondary antibody (Proteintech, China)

Table 2 PCR Primer Sequences

Target gene	Forward primer (5'-3')	Reverse primer (5'-3')
GAPDH	TGTCTCCTGCGACTTCAACA	GGTGGTCCAGGGTTTCTTACT
ALP	GCACCTGCCTTACCAACTCT	GTGGAGACGCCCATACCATC
COL I	CCCTGGTCCCTCTGGAAATG	GGACCTTTGCCCCCTTCTTT
OCN	TCTGACCTCACAGATGCCAAG	AGGGTTAAGCTCACACTGCT
RUNX2	CAGGCAGTTCCCAAGCATTT	GGTAAAGGTGGCTGGGTAGT

at room temperature for 1 hour. After the membranes were washed, an enhanced chemiluminescence (ECL) chromogenic substrate (Biyuntian, China) was used to detect the immunoreactive bands. GAPDH was used as the internal standard. The density data were quantified using ImageJ software (NIH, USA).

In vitro Antibacterial Activity

Gram-positive *Staphylococcus aureus* (Sa) (ATCC 6538; Guangdong Provincial Microbial Culture Preservation Center, China) and gram-negative *Escherichia coli* (*E. coli*) (CMCC44102; Beijing North Weiye Institute of Metrology and Nutrition, China) were used as experimental bacteria. The TI, TICU, NSPTI and NSPTICU materials were disinfected with UV radiation and placed into 48-well plates. *Staphylococcus aureus* or *Escherichia coli* suspensions of 40 μL 10^6 CFU/mL were absorbed onto the material respectively, so that the suspensions covered the surface of the material and did not drip due to tension. Then, the 48-well plates were cultured in a 37°C incubator for 1, 6, 15 or 24 h. After arriving at the time point, the materials were removed and placed in a 1.5 mL centrifuge tube. After shaking and mixing, the plates were placed in a 37°C constant temperature incubator for 18–24 hours and then the cells were counted. The sample size for each group was 6.

In vivo Animal Experiments

Twenty-four male Sprague–Dawley (SD) rats (8w, 250–300g, Vitong Lihua Co., Ltd., China) were randomly divided into four groups (TI, TICU, NSPTI and NSPTICU), with 6 rats in each group. The animal experiments were approved by the Ethics Committee of the Stomatology Hospital of Shandong University (Approval number: 20220802). All operations comply with the National Institutes of Health Laboratory Animal Care and Use Guidelines. The experimental rats were cultured in a 12/12 hour diurnal cycle culture system. Before the experiment, the rats were adaptive fed for three days.

In vivo Implantation Procedures

Prior to implantation, inhaled anesthesia was administered with isoflurane (Rayward, China), followed by intraperitoneal injection of 10% chloral hydrate solution (Comio, China). After anesthesia, the operative area of the rat was shaved and disinfected with iodophor. An incision approximately 1–2 cm in length was made beside the knee joint of the rat, and the muscle tissue was bluntly separated. A 1.2 mm diameter Titanic needle was installed on an electric drill and drilled into the rat femur at the center of the femoral condyle, perpendicular to the long axis of the femur. During the preparation process, normal saline was continuously injected to cool the femur. A pipette was used to place 10 μL (1×10^6 CFU/mL) of the *S. aureus* suspension into the bone defect, and then, rod implant materials (diameter=1.2 mm, length=10 mm) were implanted. One implant was placed in each of the left and right femurs, and the ends of the materials were not situated above the condylar surface of the femur. The wound was disinfected, and then a layered counterpoint suture was applied.

The whole implantation process was carried out under sterile conditions, and all rats were able to move normally after surgery.

Evaluation of Antibacterial Properties in vivo

Samples were taken at the first and second weeks after surgery to observe the skin and wound healing on the surface of the rat femur. Then, the femurs were removed under sterile conditions, and 3 samples from each group were placed in a centrifuge tube filled with 1 mL of normal saline, mixed, and cultured in LB solid medium in an incubator for approximately 20 hours. The remaining samples were fixed with paraformaldehyde (Biosharp, China), decalcified,

dehydrated step by step, cleared with xylene, immersed in wax, paraffin-embedded and sliced continuously. HE staining (Solarbio, China) and Giemsa staining (Solarbio, China) were used to evaluate the amount of inflammatory infiltration and bacteria around the implant.

Evaluation of Osteogenic Properties in vivo

Micro-CT and VG Staining

Four weeks after the implants were placed, both sides of the femur were separated by cardiac perfusion, fixed in 4% paraformaldehyde for two days, and then flushed for 4 hours, after which micro-computed tomography (micro-CT) (PerkinElmer, Germany) scanning was performed. The voltage was 90 kV, and the current was 88 μA. Each sample was scanned for 14 min. Mimix software was used for 3D reconstruction, and CTAn software (Bruker, Germany) was used to analyze the extent of bone repair in the area of interest around the bone defect. The main analysis indices were bone volume/tissue volume, namely, the bone volume fraction (BV/TV), bone trabecular number (Tb.N) and bone trabecular thickness (Tb.Th). GraphPad software was used for analysis and visualization. After scanning, three femur samples from each group were directly sliced into nondecalcified bone tissue sections, and van Gieson (VG) (Sigma, USA) staining was performed to determine bone area ratio (BA). BA was calculated as the area percentage of bone tissue to the whole area, which was defined as a ring extending 100 μm from the implant surface.[46]

Histological Staining

Four weeks after implantation, samples were collected. After two days of fixation with 4% paraformaldehyde, the implants were rinsed with running water for 4 hours and then placed in decalcification solution for decalcification until a needle could be inserted without resistance, indicating complete decalcification. Then, the implants were dehydrated in a semiautomatic table dehydrator (MICROM, Germany), and the sections were sliced at a thickness of 5 microns after xylene transparency, wax immersion and paraffin embedding. HE staining, Masson staining and immunohistochemical staining were performed on the paraffin sections to evaluate the formation of new bone and collagen fibers around the implant. Image J software was used to quantitatively analyze the results of HE staining and Masson staining, and the proportion of new bone area around the implant was calculated. Image J software was used for semi-quantitative analysis of the immunohistochemical staining results, and integrated optical density (IOD) was measured and its average optical density (AOD) was calculated. The AOD value (AOD=IOD/area) represent the level of immune response of its corresponding antigen. The measurements were repeated three times by the same experimenter, and the final data was averaged.

In vivo Long-Term Biosafety Evaluation

After 4 w of implantation, the heart, liver, spleen, lung and kidney of the rats in each group were harvested for HE staining to evaluate the toxicity of the materials in each group.

Statistical Analysis

The data from three independent experiments were analyzed using GraphPad Prism 7.0. All results are expressed as the mean ± standard error, and differences between groups were evaluated by one-way analysis of variance (ANOVA). *P* values were calculated using GraphPad Prism 7.0, and $P < 0.05$ was considered to indicate statistical significance.

Results and Discussion

Material Characterization Results

A naked-eye view of the nanosilver/PLGA coating is shown in Figure 1A. The thickness of the coating surface is uniform. Field emission scanning electron microscopy (SEM) with X-ray energy dispersion spectrometry (EDS) can be used to scan the surface of the sample point by point, observe the microstructure of the sample, and carry out quantitative and qualitative analysis of the elements. This technique has the advantages of fast analysis speed, accurate fixed-point analysis of microregions and simultaneous line and surface scanning analysis.[47] The SEM results showed (Figure 1B) that the silver nanoparticles were uniformly distributed in the nanosilver/PLGA coatings on the surfaces of the NSPTI

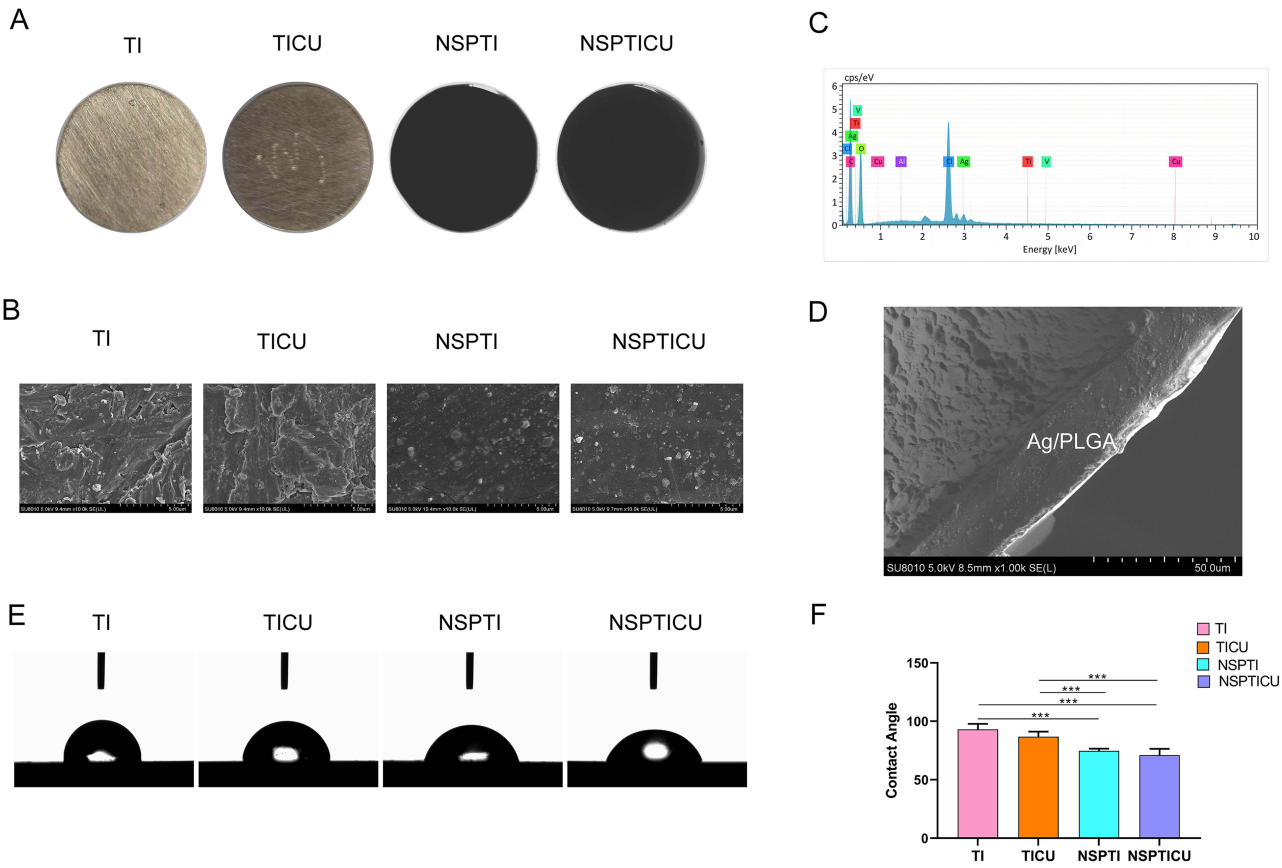

Figure 1 Characteristics of coatings.

Notes: (**A**) Material general view. (**B**) Field emission scanning electron microscopy were used to observe the surface morphology of each group; scale bar: 5 μm. (**C**) EDS elemental analysis. (**D**) SEM image showing the coating thickness of the material cross-section; scale bar: 50 μm. (**E**) and (**F**) Contact angle analysis of each group of material surfaces. ***P<0.001.

and NSPTICU, and no obvious clusters of silver nanoparticles were observed. The EDS results showed the presence of Ag in the coating, and the elemental composition and content of the nanosilver/PLGA coating are shown in Figure 1C and Table 3. Ag accounted for approximately 1.84%, which was basically consistent with our predesigned Ag content, preliminarily indicating that the nanosilver was successfully coated on the surface of the material and it could be used for subsequent experiments. In addition, the thickness of the coating is also very important for surface modification of the implant. The coating thickness of the cross-sections observed by SEM is shown in Figure 1D, and the thickness of the nanosilver/PLGA coating was approximately 32.62±2.98 μm.

Hydrophilic Evaluation of the Materials

The hydrophilicity of a material plays an important role in its interaction with cells. An increase in the surface hydrophilicity of materials can enhance cell behaviors such as cell adhesion, proliferation and differentiation.[48] To assess whether the nanosilver/PLGA coating improved the hydrophilicity of the substrate, we measured the water contact angle on the surface of the four groups of materials. PLGA is a kind of hydrophobic polymer material.[48–50] For implants used to repair defects, hydrophobic materials inhibit cell adhesion and hinder tissue growth. As a relatively hydrophilic material, nanosilver can

Table 3 Chemical Composition (Wt%) of the Nanosilver/PLGA Coatings

Element	C	O	Cl	Cu	Al	Ag
2%NSPTICU	52.71	36.75	8.62	0.05	0.02	1.84

reduce the contact angle, increase the surface wettability, and show good affinity for tissue cells,[51–53] which can compensate for the disadvantages of PLGA itself. As shown in Figure 1E and F, the contact angle of Ti was 93.05±1.96°, that of TICU was 86.75±1.81°, that of NSPTI was 74.72±0.78°, and that of NSPTICU was 71.00±2.21°, indicating that due to the addition of hydrophilic nanosilver, the hydrophilicity of the coated NSPTI and NPTICU groups improved, and there was a significant difference between the coated group and the uncoated group ($P<0.001$). However, there was no significant difference between the NSPTI and NSPTICU groups or between the TI and TICU groups ($P > 0.05$). An increase in hydrophilicity is important for enhancing the biological activity of the material, which is conducive to the adhesion and proliferation of cells on the surface of the scaffold so that it can better exert its function.[54]

In vitro Cytotoxicity Detection

Good biocompatibility is an essential feature of orthopedic biomaterials. Cell adhesion and subsequent cell proliferation and differentiation are decisive factors in determining the biocompatibility of engineered materials.[55]

We used a CCK-8 assay and live/dead cell staining to evaluate the cytotoxicity and cell proliferation capacity of the different materials. The results of the CCK-8 assay are shown in Figure 2A. On the third day, the cell proliferation of the NSPTI and NSPTICU groups was significantly greater than that of the uncoated titanium and titanium copper groups, indicating that AgNPs/PLGA promoted cell proliferation, which was consistent with the results of Liu et al.[56] This finding may be attributed to the addition of the AgNPs, which reduced the contact angle of the material and is more conducive to cell adhesion and aggregation. Alternatively, AgNPs may promote the proliferation of MC3T3 cells at noncytotoxic concentrations. On the fifth day, the proliferation of NSPTICU-treated cells was greater than that of NSPTI-treated cells, which may be related to the release of Cu^{2+}. On day 7, the proliferative activity of the NSPTICU group was the highest, and the difference was statistically significant compared with that of the other three groups, which may be due to the synergistic effect of AgNPs and Cu ions on cell proliferation. There was no significant difference between the TI, TICU and NSPTI groups ($P> 0.05$). These findings have important implications for tissue engineering.

After calcein-AM/PI staining, the live cells fluoresce green, and the dead cells fluoresce red; therefore, we visually observed the cell adhesion on each group of materials using live cell/dead cell fluorescence staining. The live/dead staining results are shown in Figure 2B. The MC3T3-E1 cells in all groups exhibited mostly green fluorescence and rarely red fluorescence, indicating good biocompatibility; this further indicates that NSPTICU has good cytocompatibility and that the introduction of AgNPs and Cu ions does not cause toxicity to cells.

In vitro Osteogenic Performance Test Results

An ideal orthopedic biomaterial should not only have good biocompatibility but also have excellent osteogenic properties at its surface/interface.[57] ALP activity is an important indicator for detecting the early differentiation of osteoblasts induced by materials.[58] Therefore, we used ALP staining and quantitative analysis of ALP activity to evaluate the early in vitro osteoinductivity of the NSPTICU. The ALP staining results are shown in Figure 3A, and the positive staining area of the same group of materials increased in a time-dependent manner from 7 days to 14 days. More significantly, the number of ALP-positive regions in the TI, TICU, NSPTI and NSPTICU increased sequentially at the same time points. The results of the quantitative analysis of ALP activity are shown in Figure 3B. At the same time, the ALP activity in the NSPTICU group was the highest, which was completely consistent with the results of the ALP staining. These results suggest that NSPTICU promotes osteogenic differentiation at an early stage. The introduction of AgNPs and copper ions improved the bone induction performance of the material in the early stage.

The degree of extracellular matrix (ECM) mineralization in MC3T3-E1 cells reflects the role of the ECM in late osteogenic differentiation.[59] We detected the degree of ECM mineralization in MC3T3-E1 cells by Alizarin red S staining to observe the late osteogenic ability of the various coatings. The results are shown in Figure 3C. Fourteen days after osteogenic induction, calcified deposits began to form on the surface of the two groups of coating materials (NSPTI, NSPTICU). Twenty-one days after osteogenic induction, a few calcified nodules were observed on the surface of the TICU alloy due to the release of Cu ions, which promoted cell osteogenesis to a certain extent. There were more mineralized nodules in the coated NSPTI group than in the TICU group, indicating that the osteogenic effect of silver nanoparticles was superior to that of copper, and the most mineralized nodules were found on the surface of NSPTICU,

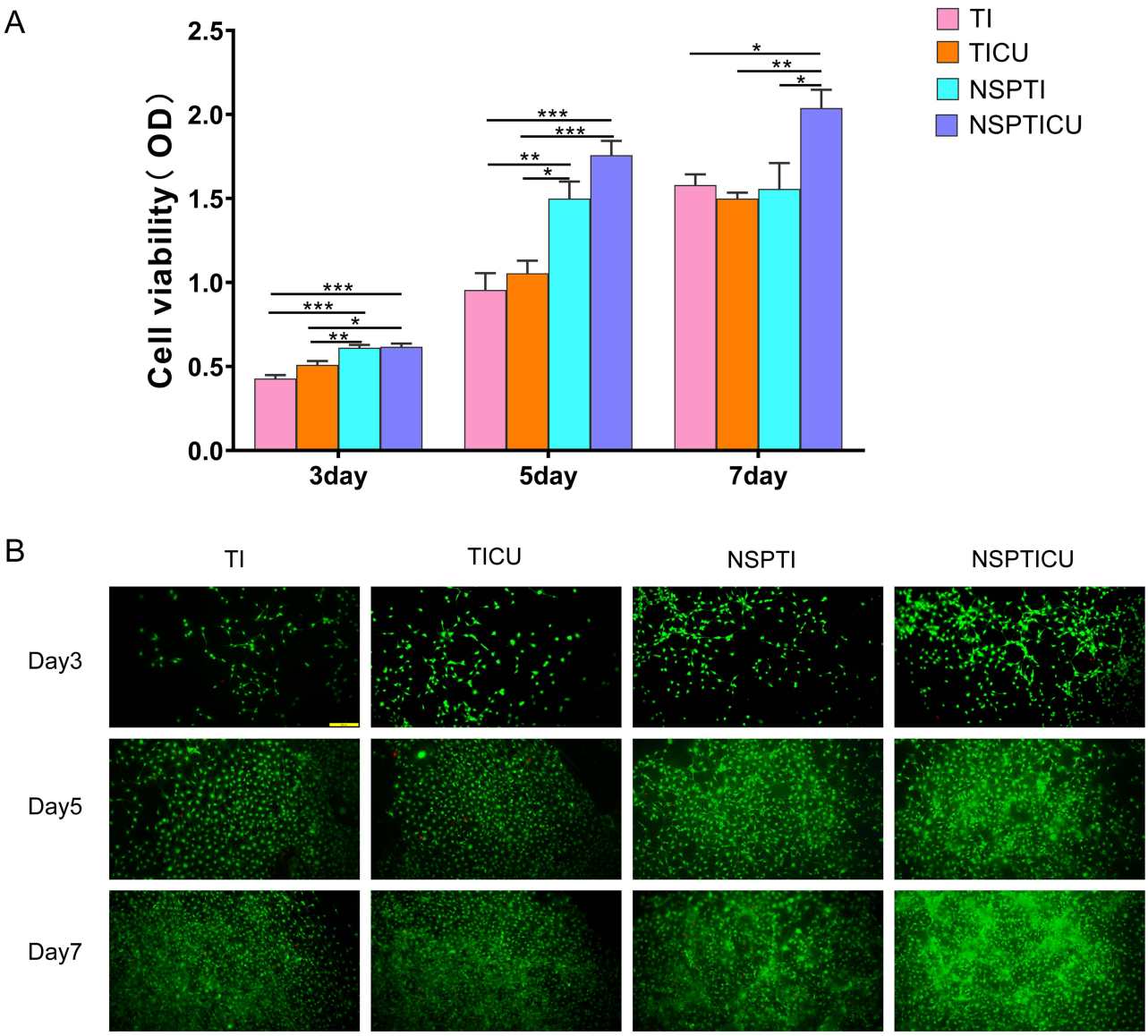

Figure 2 (**A**) MC3T3-E1 cells were cocultured with TI, TICU, NSPTI or NSPTICU implant materials for 3, 5 or 7 days, and their proliferation was detected by a CCK-8 assay. (**B**) Fluorescence images of calcein-AM/PI staining of MC3T3-E1 cells.
Notes: (**A**) **P*<0.05, ***P*<0.01, ****P*<0.001. (**B**) Scale bar: 200 μm.

which was due to the dual action of silver nanoparticles and copper ions, which accelerated cell osteogenesis. The results of the quantitative analysis of the ECM mineralization are shown in Figure 3D. Consistent with the staining results, NSPTICU had the greatest in vitro osteogenic induction ability, followed by NSPTI. These results indicate that NSPTICU also has the greatest osteogenic inductivity in the late stage of osteogenic differentiation. The addition of nanosilver and copper ions can promote the induction of late bone formation in NSPTICU. In addition, we also found that the osteogenic ability of silver nanoparticles is better than that of copper ions.

To evaluate the osteogenic differentiation ability of osteoblasts at the gene level, we investigated the mRNA expression levels of osteoblast-related genes, including ALP, COL I, RUNX2, and OCN. Many studies have confirmed that the transcription factor RUNX2 plays a crucial role in osteogenesis and can regulate the transcription of downstream genes, such as ALP, COL I, OCN.[60,61] As shown in Figure 3E, the expression levels of the RUNX2, ALP, COL I and OCN genes in the NSPTICU group were significantly greater than those in the other three groups after 7 days of osteogenic induction culture. Compared with those in the TI and TICU groups, the expression levels of RUNX2 and OCN in the NSPTI group

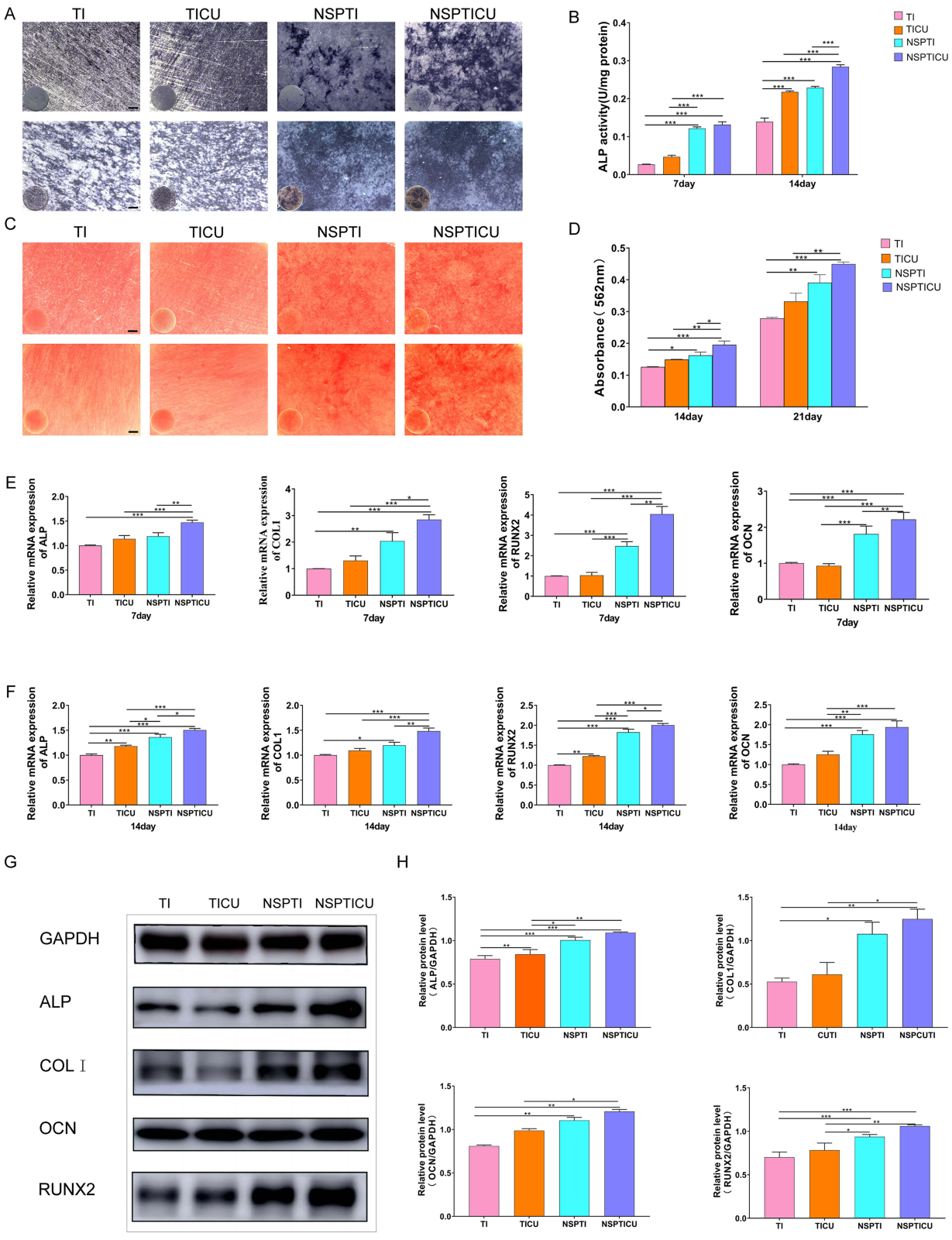

Figure 3 Results of in vitro osteogenic performance study.

Notes: (**A**) ALP staining results for each group; scale bar: 100 μm. (**B**) Quantitative results of ALP activity. (**C**) Alizarin red staining; scale bar: 100 μm. (**D**) Quantification of mineralized nodules. (**E** and **F**) The expression of the MC3T3-E1 osteogenic gene in each group was measured by qRT–PCR. (**G**) Band image of osteoblast-related protein expression. (**H**) Quantitative analysis of protein expression in each group. **P*<0.05, ***P*<0.01, ****P*<0.001.

were significantly upregulated, and the AgNPs began to exert their osteogenic effect. At this time, there was no significant difference between the TI and TICU groups, and the copper ions did not have an obvious osteogenic effect.

The results after 14 days of osteogenic induction are shown in Figure 3F. After 14 days of osteogenic induction, the NSPTI group not only exhibited upregulated expression levels of RUNX2 and OCN but also exhibited significantly upregulated expression levels of ALP and COL I, and the ratio of TI to TICU was also significantly different. It can be inferred that the silver nanoparticles fully demonstrated their osteogenic induction ability on the 14th day. At this time, compared with TI, TICU significantly upregulated the expression of ALP, RUNX2. The combination of silver nanoparticles and copper ions can promote the adhesion and aggregation of cells in the early stage and has a synergistic effect, resulting in the best osteogenic induction ability, which is highly important for bone integration after the early implantation of implants.

Finally, the expression levels of osteoblast-related proteins were further detected by Western blotting at 7 days after osteogenic induction. The results (Figure 3G) showed that the protein bands of RUNX2, ALP and COL I in the NSPTICU group were significantly deeper than those in the other three groups. Osteocalcin (OCN) is synthesized only by mature osteoblast-like cells and is an important indicator of the middle and late stages of osteogenic differentiation. The experimental results showed that there were no significant differences in the visual protein bands among the groups on day 7, which was speculated to be due to a slightly shorter induction time, and a significant difference may occur after 14 days of induction. Then, we quantitatively analyzed the obtained protein bands. As shown in Figure 3H, the expression of RUINX2, ALP, COL I, OCN in the NSPTICU group was significantly greater than that in the other three groups. The expression of RUNX2, ALP, COL I, OCN in the NSPTI group was significantly greater than that in the titanium group, but compared with those in the TICU group, only the expression of the early osteogenic proteins RUNX2 and ALP significantly differed. Compared with TI group, only the expression level of ALP was significantly increased in TICU group. In summary, NSPTICU has good biocompatibility and can promote cell proliferation.In the early stage, NSPTICU showed obvious osteogenic induction ability, followed by NSPTI, and TICU began to show osteogenic ability in the later stage.

In vitro Antibacterial Results

Staphylococcus aureus and *Escherichia coli* were used as test bacteria to evaluate the antibacterial activity of different materials against gram-positive and gram-negative bacteria. The TI, TICU, NSPTI and NSPTICU discs were cocultured with gram-positive *S. aureus* and gram-negative *E. coli* for 1 h, 6 h, 15 h or 24 h, respectively. The bacterial colonies collected from the materials of each group were diluted and counted. Based on the results (Figure 4A–D), for *Staphylococcus aureus*, titanium group materials have no antibacterial properties, and the number of bacteria gradually increases over time. Both the TICU, NSPTI and NSPTICU groups exhibited good antibacterial activity, but the antibacterial effect of the NSPTICU group was fully demonstrated at 6 hours, at which time the number of bacteria was basically 0, and at 15 hours, the number of bacteria in the NSPTI group containing the nanosilver coating was basically 0, which was significantly less than that of the TICU alloy containing the antibacterial element Cu. The results showed that the synergistic effect of silver and copper ions showed excellent antibacterial properties. In addition, we also found that the antibacterial activity of silver nanoparticles was better than that of copper ions.

For *Escherichia coli*, the results were similar to those for *Staphylococcus aureus*, the NSPTICU group had the best antibacterial performance. However, unlike *Staphylococcus aureus*, there was still a small amount of *Escherichia coli* in the NSPTICU group at 6 hours, and the number of *Escherichia coli* in the NSPTICU group was basically 0 at 15 hours. The antibacterial effect of the NSPTI group with only the nanosilver coating was better than that of the TICU group containing the element Cu. The excellent antibacterial properties of the NSPTICU group may be related to the synergistic antibacterial action of nanosilver and Cu, which is also consistent with previous research results.[62,63] The specific mechanism of synergistic antibacterial activity needs further study. In addition, we also found that NSPTICU has a better antibacterial effect against gram-positive Staphylococcus aureus than against gram-negative Escherichia coli, which is consistent with previous findings.[64]

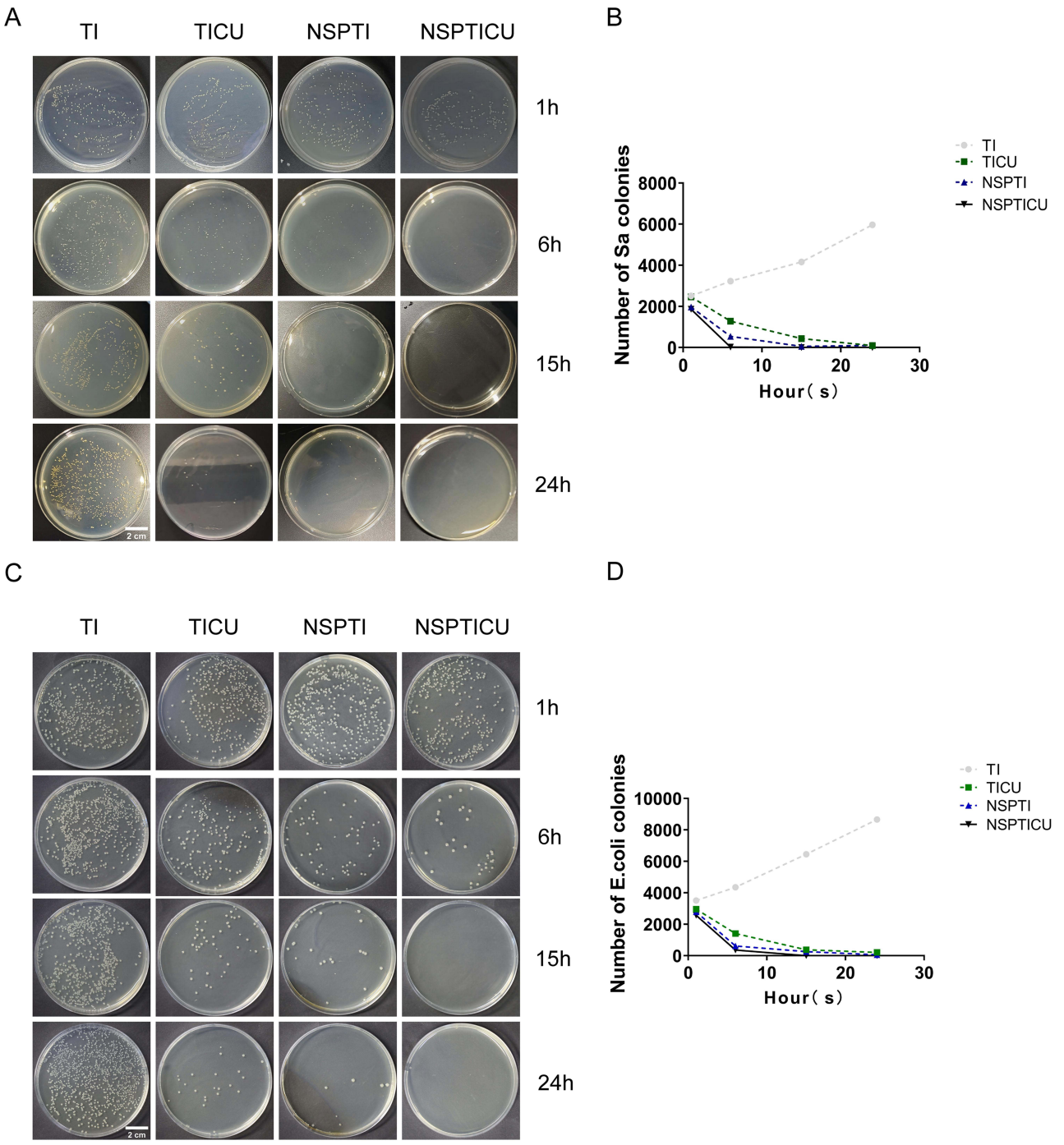

Figure 4 Antibacterial ability of different materials against *S. aureus* and *E. coli* in vitro.
Notes: (**A**) Results of coating plates with different materials cocultured with *S. aureus* (tenfold dilution of colonies). (**B**) Line chart of colony numbers of each group cocultured with *S. aureus* for 1 h, 6 h, 15 h or 24 h. (**C**) Plate coating results of different materials cocultured with *Escherichia coli* (tenfold colony dilution). (**D**) The broken line graph of the number of colonies after 1 h, 6 h, 15 h or 24 h of coculture with *Escherichia coli* and different materials. Scale bar: 2 cm.

Evaluation of Antibacterial Properties in vivo

The implantation process is shown in Figure 5A. After 1 w and 2 w of implantation, samples were taken (Figure 5B). The surface wound healing of rat femur skin containing TI implants was poor, and tissue purulence and surface swelling were observed. The femoral surface of the rats that received TICU implants was slightly red, while the femoral surface of the rats that received NSPTI and NSPTICU implants achieved good wound healing without redness, swelling or discharge of

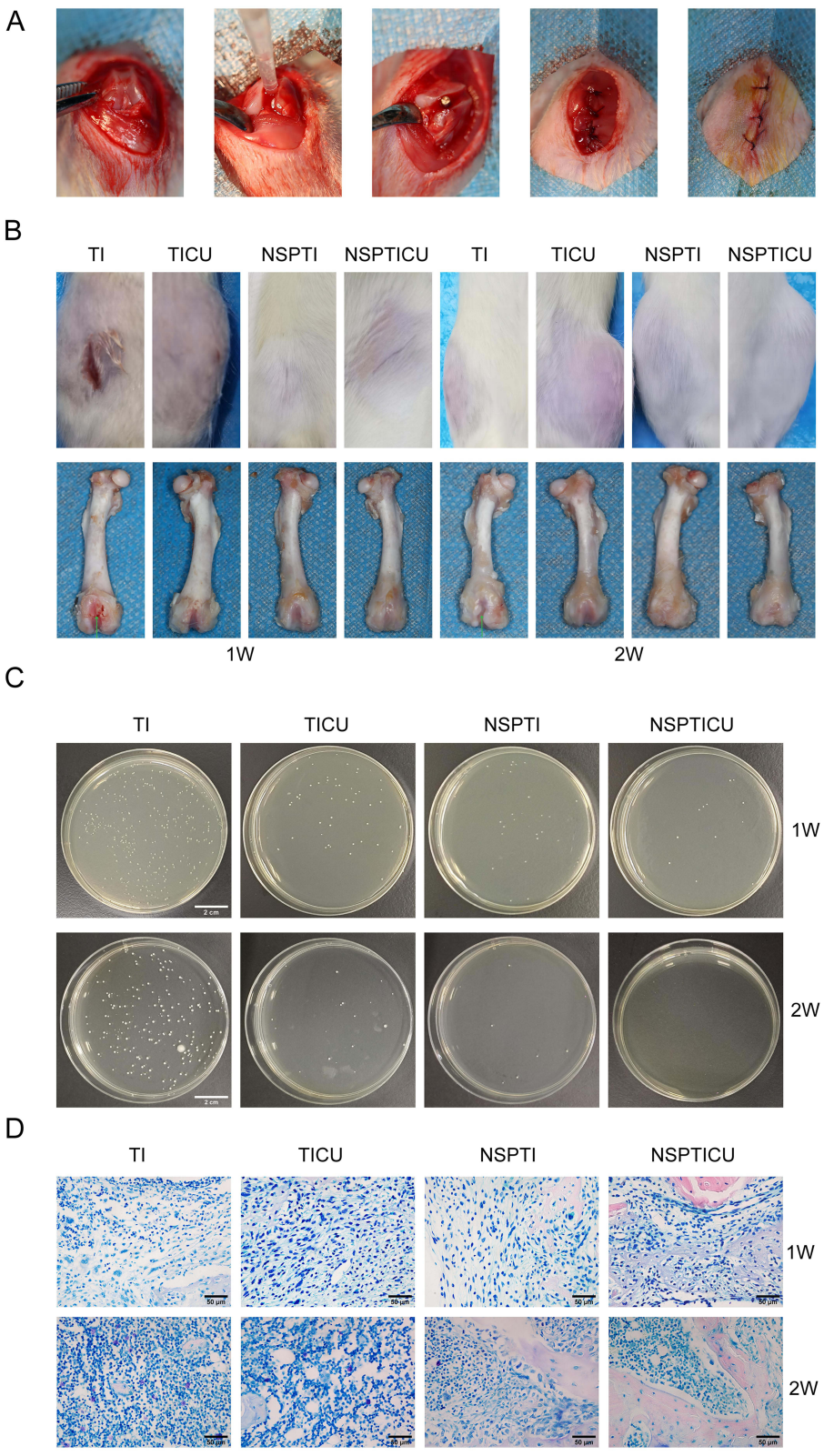

Figure 5 Evaluation of the antimicrobial activity of NSPTICU in vivo.
Notes: (**A**) The implantation procedure. (**B**) Gross view of femoral osteomyelitis in rats. The green arrow points to the implant site. (**C**) Schematic diagram of bacteria collected from the four groups of implants; scale bar: 2 cm. (**D**) Bacterial residue was observed by Giemsa staining (400×) after 1 w and 2 w of implantation in each group; scale bar: 50 μm.

pus. Through the rat femur specimen, the green arrow pointed to the site where the implant was implanted. 1 week later, it was found that the titanium implant group had partial bone defect, while the other groups did not have obvious inflammation and bone defect. Two weeks later, bone tissue deformation and pus were observed at the femoral implant in the TI group, while no significant inflammation was observed in the NSPTI and NSPTICU groups, and the bone defect around the implant was well healed. These results showed that both the NSPTICU and NSPTI coatings had good antibacterial activity, and the TICU group also had antibacterial activity comparable to that of the TI group but not to the same extent as that of the NSPPTI and NSPTICU groups.

At 1 w or 2 w, the bacterial suspension from each group was diluted 10 times and cultured on LB solid medium for 20 h. The results showed (Figure 5C) that the bacteria collected on the implants of the TI group were the most abundant, and the bacteria on the implants in the other three groups were significantly decreased compared with those of the TI group. No bacteria were present on the NSPTICU alloy implant, and its antibacterial performance was better than that of the other three groups, which was consistent with the in vitro antibacterial results. Giemsa staining (Figure 5D) was used to observe the presence of bacteria around the implant. At 1 w, many bacteria were present around the TI group, while the number of bacteria in the other three groups was lower than that in the TI group. At the 2nd week, multiple macrophages were observed around the TI implant, and macrophages were observed around the TICU implants. However, only a few macrophages were present in the NSPTI group, and no macrophages were found in the NSPTICU group. The above results also confirmed that NSPTICU has excellent antibacterial activity in vivo.

HE staining was further used to observe the inflammation of tissues around different implant materials. The results showed that in the 1st w (Figure 6A), there was obvious inflammation and bone tissue destruction around the TI implant, and more inflammatory cells could be seen around the TI implant. There were fewer inflammatory cells around the TICU and NSPTI implants than around the TI implants, and there were almost no inflammatory cells around the NSPTICU implants. In the 2nd w (Figure 6B), there were almost no inflammatory cells around the NSPTI or NSPTICU implants, and a small amount of new bone formation was observed. These results were consistent with the in vitro antibacterial results, suggesting that the three experimental groups exhibited antibacterial abilities and that the antibacterial ability of the NSPTICU group was greater than that of the other groups. In week 2 (Figure 6B), there were fewer inflammatory cells in the TICU group, and almost no inflammatory cells existed around the NSPTI and NSPTICU implants. These results were consistent with the in vitro antibacterial results. In the early stage, NSPTICU showed complete antibacterial ability, while the antibacterial efficiency of NSPTI was lower than that of NSPTICU. Although TICU had antibacterial ability, it was inferior to that of the other two groups. Based on the above results, the NSPTICU group of materials has high efficiency and excellent antibacterial and anti-inflammatory ability. The combination of two antibacterial elements (nanosilver and Cu) can result in greater efficiency and superior antibacterial ability than a single element, which has a certain reference significance for implant design to prevent implant infection.

Evaluation of Osteogenic Performance in vivo

The TI, TICU, NSPTI and NSPTICU materials were implanted into rats for 4 weeks, the femurs of each group were scanned via micro-CT, and the results were imported into Mimix for 3D reconstruction. Yellow indicates implants, and blue indicates new bone formation. Intuitively (Figure 7A), the amount of new bone formed around the NSPTICU implant was the greatest, while the amount of new bone formed around the TI implant was the lowest. The amount of new bone formation in the TICU and NSPTI groups was greater than that in the TI group but less than that in the NSPTICU group. CTAn software was used to quantitatively analyze the bone in the area of interest (0.5 mm around the implant). The results showed (Figure 7B) that the bone volume fraction (BV/TV), bone trabecular thickness (Tb.Th) and bone trabecular number (Tb.N) around the implant were arranged in the following order: NSPTICU > NSPTI > TICU > TI. The NSPTICU group significantly differed from the other three groups.

In addition, we performed H&E and Masson tricolor analyses on femur specimens to assess bone integration around different materials. As shown in Figure 7C, H&E staining revealed that a small amount of new bone was formed near the implant in the titanium group, more new bone was formed in the TICU group than in the TI group, and a large amount of new bone appeared around the NSPTI and NSPTICU groups, while the most complete and thickest new bone matrix was formed around the NSPTICU group. According to Figure 7D, NSPTICU group accounted for the highest proportion of

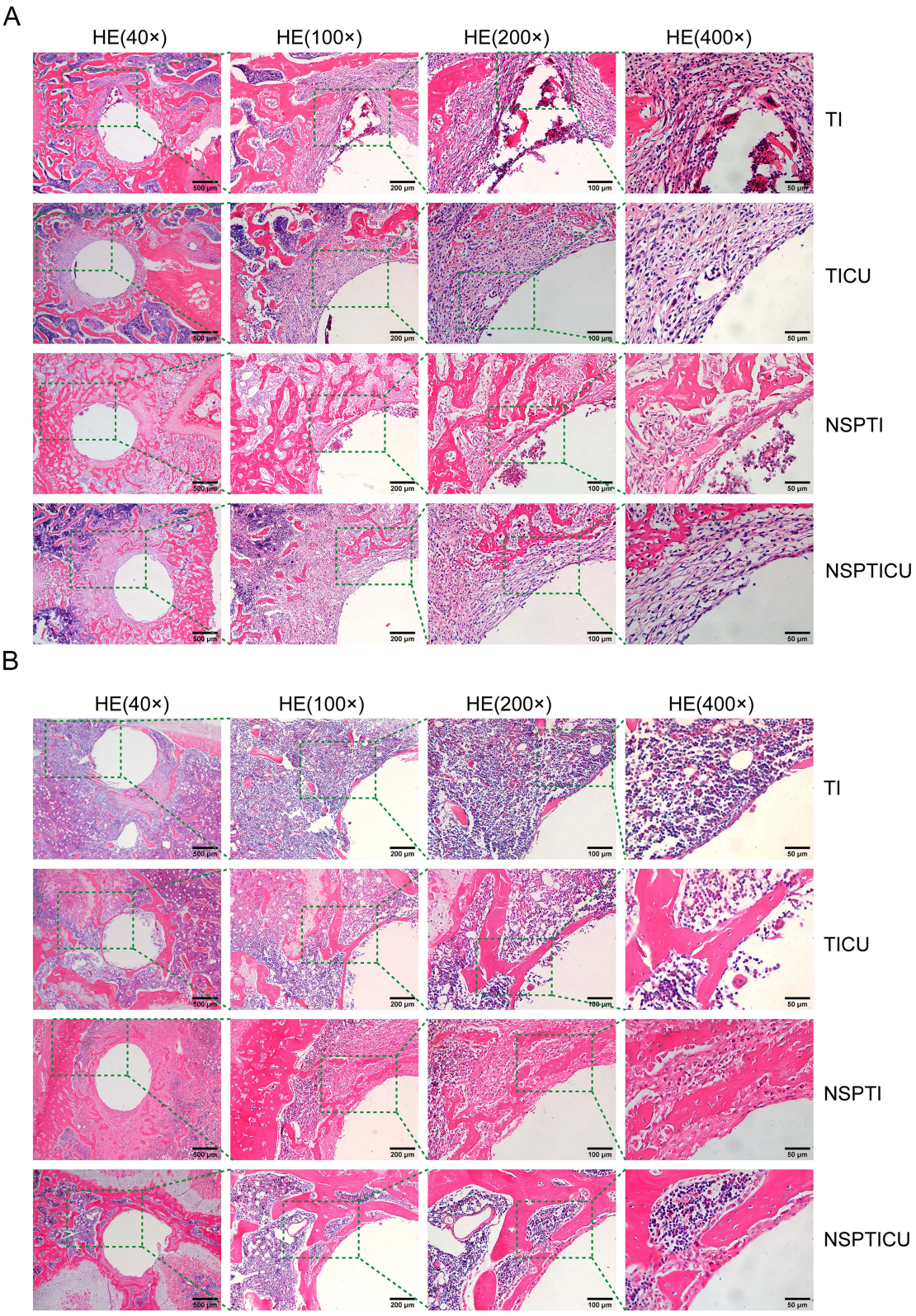

Figure 6 (**A**) After 1 w of implantation. (**B**) Two weeks after implantation.
Notes: (**A**) HE staining was performed to observe inflammatory cell infiltration around the implant from whole to local. (**B**) HE staining was performed to observe the infiltration of inflammatory cells around the implants; scale bar: 500 μm/200 μm/100 μm/50 μm.

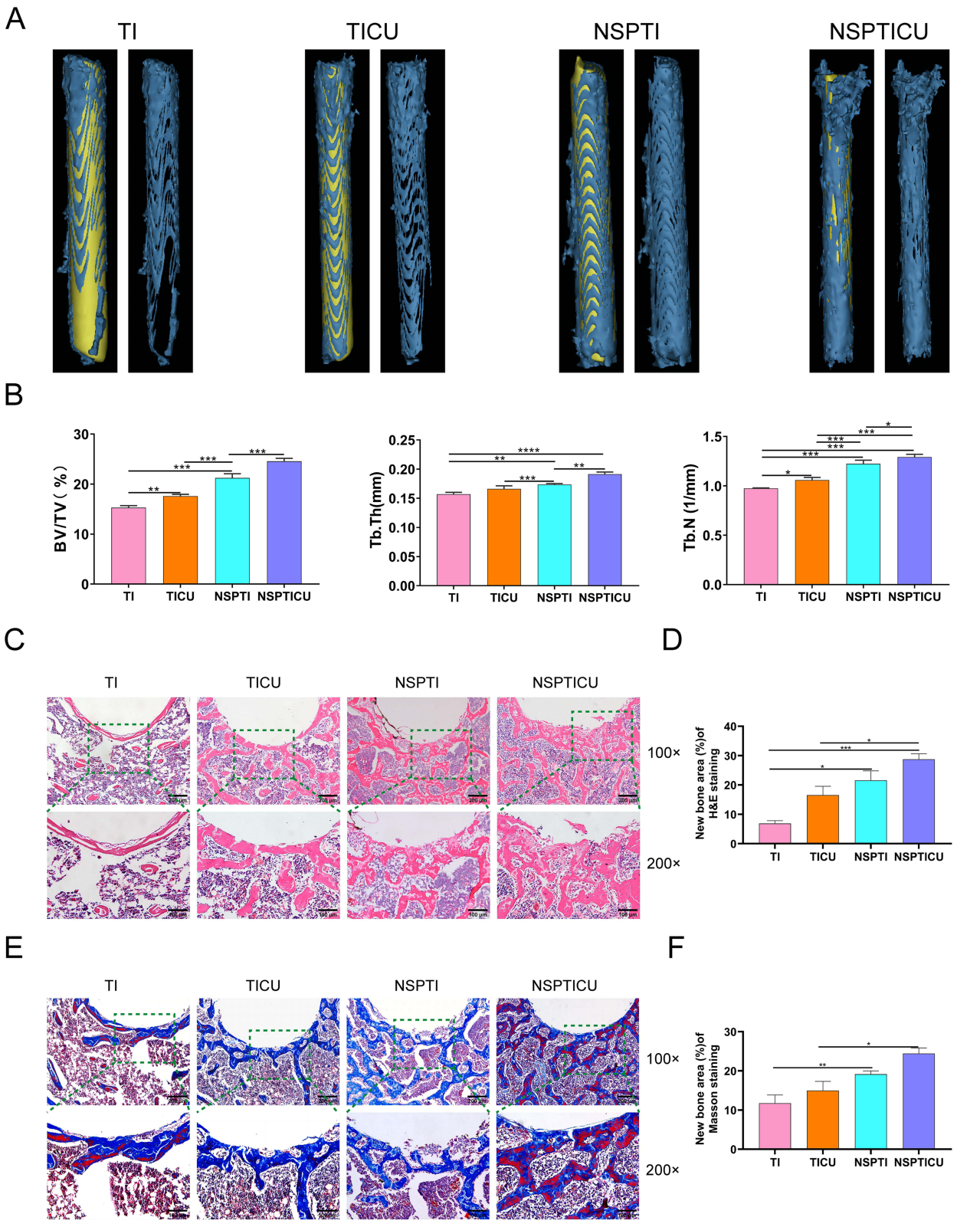

Figure 7 Evaluation of the osteogenic properties of NSPTICU in vivo.

Notes: (**A**) After 4 w of implant implantation, 3D micro-CT images of the different groups were reconstructed. (**B**) Bone metrological analysis of the of interest around the implants in the 4 groups (**P*<0.05; ***P*<0.01; ****P*<0.001). (**C**) HE staining of bone tissue around the implant. (**D**) Quantitative analysis of new bone tissue area in each group stained by HE. (**P*<0.05, ****P*<0.001, mean ± SEM, n=3). (**E**) Masson staining of bone regeneration around implants at 4 weeks after surgery. Scale bar: 200 μm/100 μm. (**F**) Quantitative analysis of tissue area of new bone in each group with Masson staining. (**P*<0.05, ***P*<0.01, mean ± SEM, n=3).

new bone area (28.8%), followed by NSPTI (21.6%), TICU (16.6%) and TI (6.9%). There was statistical significance between NSPTICU group and TI and TICU group.

Masson staining (Figure 7E) revealed that the number of bone trabeculae around the implants in the TI group was small and discontinuous, with less new bone formation, while the number of bone trabeculae in the NSPTI and NSPTICU groups was significantly greater, but the bone matrix around the implants in the NSPTICU group seemed to be more mature, dense and continuous. In Figure 7F, the percentage of new bone-like tissue area stained by Masson was also the highest in NSPTICU group (24.4%). These results indicate that the NSPTICU implant has better bone induction ability.

In addition, 4 weeks after implantation, hard tissue sections were used to observe bone formation around the implants in each group. The VG staining results are shown in Figure 8A, in which black represents the implant and red represents the surrounding bone tissue. Consistent with the above experimental results, the amount of new bone formed decreased in the following order: NSPTICU > NSPTI > TICU > TI. As shown in Figure 8B, the BA results showed that the bone formation area around the NSPTICU implant had the highest proportion (21.3%), followed by the NSPTI group (19.3%).

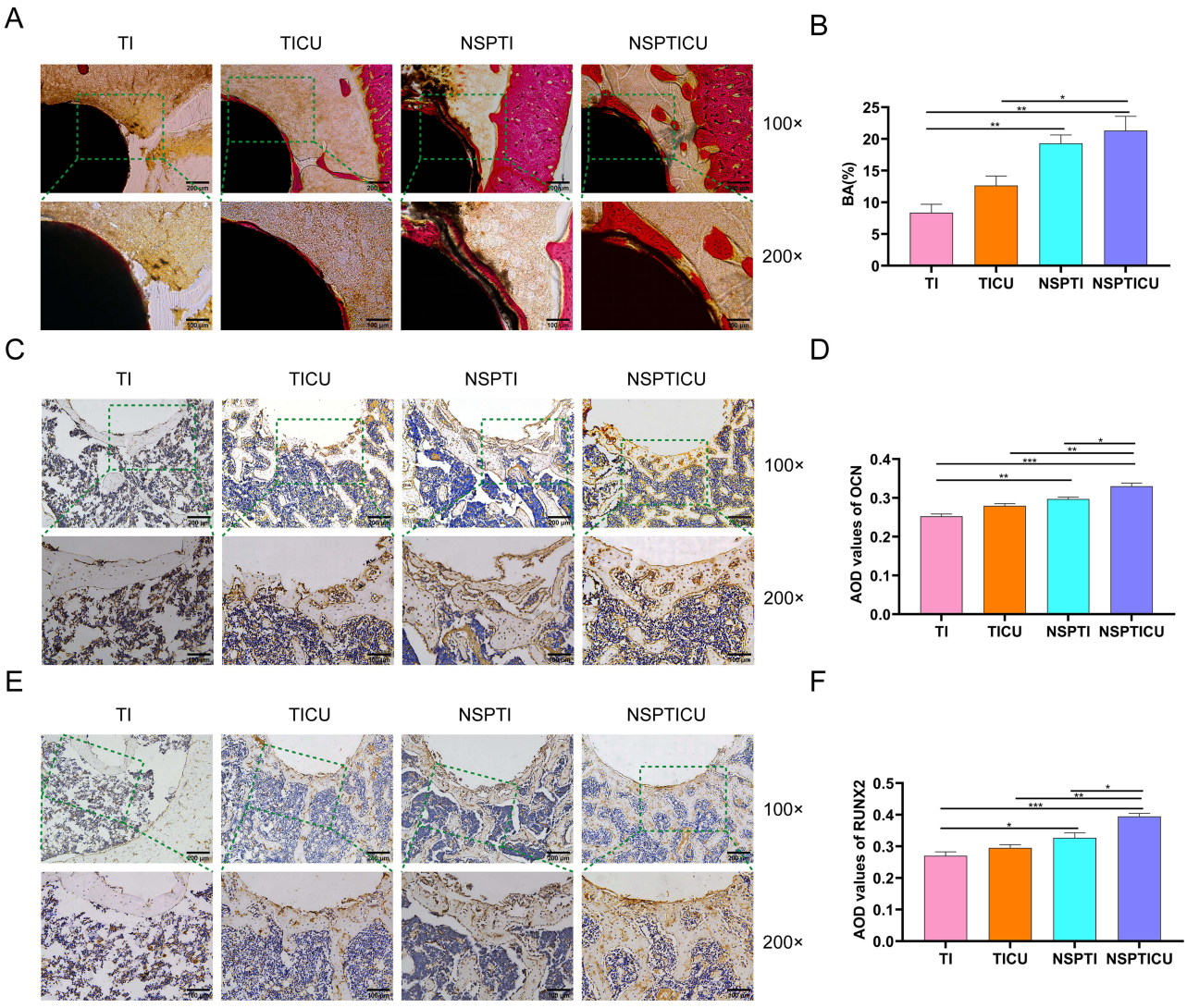

Figure 8 Evaluation of osteogenic properties of each group of materials in vivo.

Notes: (**A**) VG staining of hard tissue sections of different samples. (**B**) Quantification of newly formed bone area ratio (BA) within 100 μm from the implant surfaces using imageJ software. (**P*<0.05, ***P*<0.01, mean ± SEM, n=3). (**C**) Immunohistochemical staining of OCN around each implant. Scale bar: 200 μm/100 μm. (**D**) AOD values of OCN (**P*<0.05, ***P*<0.01, ****P*<0.001, mean ± SEM, n=3). (**E**) Immunohistochemical staining of RUNX2 around each implant. Scale bar: 200 μm/100 μm. (**F**) AOD values of RUNX2 (**P*<0.05, ***P*<0.01, ****P*<0.001, mean ± SEM, n = 3).

https://doi.org/10.2147/IJN.S456906 DovePress

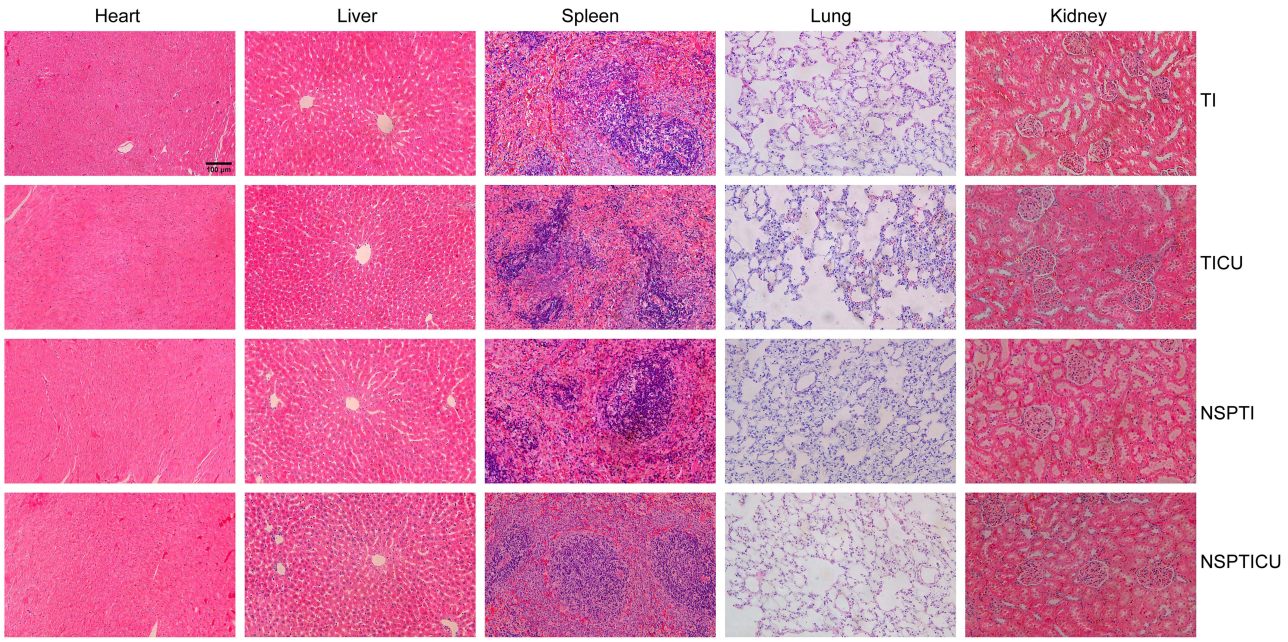

Figure 9 HE staining analysis of the heart, liver, spleen, lung and kidney of implanted rats in each group.
Note: Magnification 200×, scale bar: 100 μm.

All three experimental groups exhibited osteogenic induction ability, but the amount of new bone formed in the NSPTICU group was the greatest, and the osteogenic ability was more significant.

In addition, the expression levels of two osteogenic marker proteins, OCN and RUNX2, around the TI, TICU, NSPTI and NSPTICU implant materials were investigated by immunohistochemical staining. The results are shown in Figure 8C–F, respectively, in which the positively stained cells are brown and the nuclei are blue. The expression levels of OCN and RUNX2 were greater in the NSPTI and NSPTICU groups than in the other groups, but the expression level in the NSPTICU group was the highest.

In summary, we can conclude that NSPTICU has good antibacterial and bone integration properties in vivo and is a promising implant material.

In vivo Long-Term Safety Evaluation

Four weeks after implant placement, the heart, liver, spleen, lung and kidney of the rats in each group were removed for HE staining and observation. The results showed that normal organizational structure and morphology were visible in each group (Figure 9). No obvious pathological changes were observed, indicating that the implants in the NSPTICU exhibit good biological safety. Metal ion or metal nanoparticle antimicrobials have broad-spectrum antibacterial activity and multiple antibacterial mechanisms, but their high-dose application is usually cytotoxic. We preliminarily confirmed that the 2% AgNPs/PLGA coating has good biocompatibility when added to TI6AL4V-CU through in vitro CCK-8 and live/dead cell staining experiments, and in vivo experiments also confirmed its safety.

Conclusion

In this study, nanosilver/PLGA was coated on TI6AL4V-CU by solvent casting method to construct a new type of antibacterial and osteogenic NSPTICU implant with synergistic effect of nanosilver and copper ions, which can be used to prevent infection and promote bone formation in bone defect repair. This method has the advantages of simple preparation process and low cost. The results show that the NSPTICU coating has good hydrophilicity when silver nanoparticles are uniformly coated on the surface of titanium-copper alloy. NSPTICU has the ability to release silver and copper ions, and has significant synergistic antibacterial action against both gram-positive *Staphylococcus aureus* and gram-negative *Escherichia coli*. In addition, due to the clever introduction of silver nanoparticles and copper ions, they

also have a synergistic effect on bone induction, making NSPTICU show excellent bone induction ability both in vivo and in vitro. In summary, under the synergistic action of Ag and Cu, the antibacterial and bone integration properties of Ti surface reached a balance. The dual-function coating has a good application prospect in the repair of infected bone defects in clinic.

Data Sharing Statement

The datasets used and/or analyzed during the current study are available from the corresponding author upon reasonable request.

Ethics Approval and Consent to Participate

All animal experimental procedures were approved by the Animal Ethics Committee of Shandong University School of Stomatology (No.20220802) and carried out in accordance with the UK Animals (Scientific Procedures) Act (1986).

Acknowledgments

This work was financially supported by the National Natural Science Foundation of China (No. 81701008), Natural Science Foundation of Shandong Province, China (No. ZR2023MH199), Key research and development program of Shandong Province, China (No. 2019GSF108187), and Special funds for Taishan Scholars Project of Shandong Province, China (No. tsqn202306367). We thank Professor Ling Ren from Institute of Metal Research, Chinese Academy of Sciences, China for providing us with the TI6AL4V-CU materials.

Disclosure

The authors report no conflicts of interest in this work.

References

1. Wu S, Xu J, Zou L, et al. Long-lasting renewable antibacterial porous polymeric coatings enable titanium biomaterials to prevent and treat peri-implant infection. *Nat Commun*. 2021;12(1):3303. doi:10.1038/s41467-021-23069-0
2. Souza JCM, Sordi MB, Kanazawa M, et al. Nano-scale modification of titanium implant surfaces to enhance osseointegration. *Acta Biomater*. 2019;94:112–131. doi:10.1016/j.actbio.2019.05.045
3. Wu H, Chen X, Kong L, Liu P. Mechanical and biological properties of titanium and its alloys for oral implant with preparation techniques: a review. *Materials*. 2023;16(21). doi:10.3390/ma16216860
4. Zhang YF, Gulati K, Li Z, Di P, Liu Y. Dental implant nano-engineering: advances, limitations and future directions. *Nanomaterials*. 2021;11(10):26.
5. Parthasarathy J, Starly B, Raman S, Christensen A. Mechanical evaluation of porous titanium (Ti6Al4V) structures with electron beam melting (EBM). *J Mech Behav Biomed Mater*. 2010;3(3):249–259. doi:10.1016/j.jmbbm.2009.10.006
6. Diamanti MV, Del Curto B, Pedeferri M. Anodic oxidation of titanium: from technical aspects to biomedical applications. *J Appl Biomater Biomech*. 2011;9(1):55–69. doi:10.5301/JABB.2011.7429
7. Zhang W, Wang G, Liu Y, et al. The synergistic effect of hierarchical micro/nano-topography and bioactive ions for enhanced osseointegration. *Biomaterials*. 2013;34(13):3184–3195. doi:10.1016/j.biomaterials.2013.01.008
8. Zhou R, Han Y, Cao J, et al. Enhanced osseointegration of hierarchically structured ti implant with electrically bioactive SnO_2-TiO_2 bilayered surface. *ACS Appl Mater Interfaces*. 2018;10(36):30191–30200. doi:10.1021/acsami.8b10928
9. Wang B, Wu Z, Wang S, et al. Mg/Cu-doped TiO_2 nanotube array: a novel dual-function system with self-antibacterial activity and excellent cell compatibility. *Mater Sci Eng C Mater Biol Appl*. 2021;128:112322. doi:10.1016/j.msec.2021.112322
10. Bakhshandeh S, Gorgin Karaji Z, Lietaert K, et al. Simultaneous delivery of multiple antibacterial agents from additively manufactured porous biomaterials to fully eradicate planktonic and adherent staphylococcus aureus. *ACS Appl Mater Interfaces*. 2017;9(31):25691–25699. doi:10.1021/acsami.7b04950
11. Wang B, Lan J, Qiao H, et al. Porous surface with fusion peptides embedded in strontium titanate nanotubes elevates osteogenic and antibacterial activity of additively manufactured titanium alloy. *Colloids Surf B Biointerfaces*. 2023;224:113188. doi:10.1016/j.colsurfb.2023.113188
12. Zeng J, Gu C, Geng X, Lin K, Xie Y, Chen X. Combined photothermal and sonodynamic therapy using a 2D black phosphorus nanosheets loaded coating for efficient bacterial inhibition and bone-implant integration. *Biomaterials*. 2023;297:122122. doi:10.1016/j.biomaterials.2023.122122
13. Li X, Xu M, Geng Z, et al. Novel pH-responsive CaO_2@ZIF-67-HA-ADH coating that efficiently enhances the antimicrobial, osteogenic, and angiogenic properties of titanium implants. *ACS Appl Mater Interfaces*. 2023;15(36):42965–42980. doi:10.1021/acsami.3c08233
14. Raphel J, Holodniy M, Goodman SB, Heilshorn SC. Multifunctional coatings to simultaneously promote osseointegration and prevent infection of orthopaedic implants. *Biomaterials*. 2016;84:301–314. doi:10.1016/j.biomaterials.2016.01.016
15. Li X, Yang B, Xu M, et al. Doped multiple nanoparticles with hydroxyapatite coating show diverse health effects in vivo. *Int J Nanomed*. 2023;18:5031–5054. doi:10.2147/IJN.S417929

16. Zhang F, Zhang Z, Zhu X, Kang ET, Neoh KG. Silk-functionalized titanium surfaces for enhancing osteoblast functions and reducing bacterial adhesion. *Biomaterials*. 2008;29(36):4751–4759. doi:10.1016/j.biomaterials.2008.08.043
17. Campoccia D, Montanaro L, Arciola CR. The significance of infection related to orthopedic devices and issues of antibiotic resistance. *Biomaterials*. 2006;27(11):2331–2339. doi:10.1016/j.biomaterials.2005.11.044
18. Donlan RM, Costerton JW. Biofilms: survival mechanisms of clinically relevant microorganisms. *Clin Microbiol Rev*. 2002;15(2):167–193. doi:10.1128/CMR.15.2.167-193.2002
19. Vepari C, Kaplan DL. Silk as a Biomaterial. *Prog Polym Sci*. 2007;32(8–9):991–1007. doi:10.1016/j.progpolymsci.2007.05.013
20. Wang Y, Kim H-J, Vunjak-Novakovic G, Kaplan DL. Stem cell-based tissue engineering with silk biomaterials. *Biomaterials*. 2006;27 (36):6064–6082. doi:10.1016/j.biomaterials.2006.07.008
21. Dalsin JL, Hu BH, Lee BP, Messersmith PB. Mussel adhesive protein mimetic polymers for the preparation of nonfouling surfaces. *J Am Chem Soc*. 2003;125(14):4253–4258. doi:10.1021/ja0284963
22. Zhao L, Hu Y, Xu D, Cai K. Surface functionalization of titanium substrates with chitosan-lauric acid conjugate to enhance osteoblasts functions and inhibit bacteria adhesion. *Colloids Surf B Biointerfaces*. 2014;119:115–125. doi:10.1016/j.colsurfb.2014.05.002
23. Cao H, Zhang W, Meng F, et al. Osteogenesis catalyzed by titanium-supported silver nanoparticles. *ACS Appl Mater Interfaces*. 2017;9 (6):5149–5157. doi:10.1021/acsami.6b15448
24. Zhang R, Lee P, Lui VC, et al. Silver nanoparticles promote osteogenesis of mesenchymal stem cells and improve bone fracture healing in osteogenesis mechanism mouse model. *Nanomedicine*. 2015;11(8):1949–1959. doi:10.1016/j.nano.2015.07.016
25. Manjumeena R, Duraibabu D, Sudha J, Kalaichelvan PT. Biogenic nanosilver incorporated reverse osmosis membrane for antibacterial and antifungal activities against selected pathogenic strains: an enhanced eco-friendly water disinfection approach. *J Environ Sci Health Part A*. 2014;49(10):1125–1133.
26. Sanpui P, Murugadoss A, Prasad PVD, Ghosh SS, Chattopadhyay A. The antibacterial properties of a novel chitosan-Ag-nanoparticle composite. *Int J Food Microbiol*. 2008;124(2):142–146. doi:10.1016/j.ijfoodmicro.2008.03.004
27. Ravichandran R, Ng CC, Liao S, et al. Biomimetic surface modification of titanium surfaces for early cell capture by advanced electrospinning. *Biomed Mater*. 2012;7(1):16. doi:10.1088/1748-6041/7/1/015001
28. Garg T, Rath G, Goyal AK. Biomaterials-based nanofiber scaffold: targeted and controlled carrier for cell and drug delivery. *J Drug Target*. 2015;23 (3):202–221. doi:10.3109/1061186X.2014.992899
29. Almajhdi FN, Fouad H, Khalil KA, et al. In-vitro anticancer and antimicrobial activities of PLGA/silver nanofiber composites prepared by electrospinning. *J Mater Sci-Mater Med*. 2014;25(4):1045–1053. doi:10.1007/s10856-013-5131-y
30. Wei YJ, Liu ZQ, Zhu X, et al. Dual directions to address the problem of aseptic loosening via electrospun PLGA @ aspirin nanofiber coatings on titanium. *Biomaterials*. 2020;257:14. doi:10.1016/j.biomaterials.2020.120237
31. Gentile P, Chiono V, Carmagnola I, Hatton PV. An overview of poly(lactic-co-glycolic) acid (PLGA)-based biomaterials for bone tissue engineering. *Int J Mol Sci*. 2014;15(3):3640–3659. doi:10.3390/ijms15033640
32. Zhuang YF, Zhang SY, Yang K, Ren L, Dai KR. Antibacterial activity of copper-bearing 316L stainless steel for the prevention of implant-related infection. *J Biomed Mater Res Part B*. 2020;108(2):484–495. doi:10.1002/jbm.b.34405
33. Vimbela GV, Ngo SM, Fraze C, Yang L, Stout DA. Antibacterial properties and toxicity from metallic nanomaterials (vol 12, pg 3941, 2017). *Int J Nanomed*. 2018;13:6497. doi:10.2147/IJN.S183907
34. Liu R, Memarzadeh K, Chang B, et al. Antibacterial effect of copper-bearing titanium alloy (Ti-Cu) against Streptococcus mutans and Porphyromonas gingivalis. *Sci Rep*. 2016;6:10. doi:10.1038/s41598-016-0003-6
35. Sun D, Xu DK, Yang CG, et al. Inhibition of Staphylococcus aureus biofilm by a copper-bearing 317L-Cu stainless steel and its corrosion resistance. *Mater Sci Eng C-Mater Biol Appl*. 2016;69:744–750. doi:10.1016/j.msec.2016.07.050
36. Nan L, Xu DK, Gu TY, Song X, Yang K. Microbiological influenced corrosion resistance characteristics of a 304L-Cu stainless steel against Escherichia coli. *Mater Sci Eng C-Mater Biol Appl*. 2015;48:228–234. doi:10.1016/j.msec.2014.12.004
37. Ma Z, Li M, Liu R, et al. In vitro study on an antibacterial Ti-5Cu alloy for medical application. *J Mater Sci-Mater Med*. 2016;27(5):12. doi:10.1007/s10856-016-5698-1
38. Bai B, Zhang EL, Liu JC, Zhu JT. The anti-bacterial activity of titanium-copper sintered alloy against Porphyromonas gingivalis in vitro. *Dent Mater J*. 2016;35(4):659–667. doi:10.4012/dmj.2016-001
39. Zhang EL, Ren J, Li SY, Yang L, Qin GW. Optimization of mechanical properties, biocorrosion properties and antibacterial properties of as-cast Ti-Cu alloys. *Biomed Mater*. 2016;11(6):13. doi:10.1088/1748-6041/11/6/065001
40. Zhuang YF, Ren L, Zhang SY, Wei X, Yang K, Dai KR. Antibacterial effect of a copper-containing titanium alloy against implant-associated infection induced by methicillin-resistant Staphylococcus aureus. *Acta Biomater*. 2021;119:472–484. doi:10.1016/j.actbio.2020.10.026
41. Chen X, Ku S, Weibel JA, et al. Enhanced antimicrobial efficacy of bimetallic porous CuO microspheres decorated with Ag nanoparticles. *ACS Appl Mater Interfaces*. 2017;9(45):39165–39173. doi:10.1021/acsami.7b11364
42. Garza-Cervantes JA, Chavez-Reyes A, Castillo EC, et al. Synergistic antimicrobial effects of silver/transition-metal combinatorial treatments. *Sci Rep*. 2017;7(1):903. doi:10.1038/s41598-017-01017-7
43. Yan J, Xia D, Zhou W, et al. pH-responsive silk fibroin-based CuO/Ag micro/nano coating endows polyetheretherketone with synergistic antibacterial ability, osteogenesis, and angiogenesis. *Acta Biomater*. 2020;115:220–234. doi:10.1016/j.actbio.2020.07.062
44. Aguayo S, Donos N, Spratt D, Bozec L. Nanoadhesion of staphylococcus aureus onto titanium implant surfaces. *J Dent Res*. 2015;94 (8):1078–1084. doi:10.1177/0022034515591485
45. Herrero-Herrero M, Gomez-Tejedor JA, Valles-Lluch A. Role of Electrospinning Parameters on Poly(Lactic-co-Glycolic Acid) and Poly (Caprolactone-co-Glycolic acid) Membranes. *Polymers*. 2021;13(5). doi:10.3390/polym13050695
46. Cheng H, Xiong W, Fang Z, et al. Strontium (Sr) and silver (Ag) loaded nanotubular structures with combined osteoinductive and antimicrobial activities. *Acta Biomater*. 2016;31:388–400. doi:10.1016/j.actbio.2015.11.046
47. Zeng X, Xiong S, Zhuo S, et al. Nanosilver/poly (dl-lactic-co-glycolic acid) on titanium implant surfaces for the enhancement of antibacterial properties and osteoinductivity. *Int J Nanomed*. 2019;14:1849–1863. doi:10.2147/IJN.S190954
48. Chen L, Shao L, Wang F, Huang Y, Gao F. Enhancement in sustained release of antimicrobial peptide and BMP-2 from degradable three dimensional-printed PLGA scaffold for bone regeneration. *RSC Adv*. 2019;9(19):10494–10507. doi:10.1039/C8RA08788A

49. Ellinas K, Tserepi A, Gogolides E. Durable superhydrophobic and superamphiphobic polymeric surfaces and their applications: a review. *Adv Colloid Interface Sci*. 2017;250:132–157. doi:10.1016/j.cis.2017.09.003
50. Sun Y, Jia X, Meng Q. Characteristic evaluation of recombinant MiSp/Poly(lactic-co-glycolic) Acid (PLGA) nanofiber scaffolds as potential scaffolds for bone tissue engineering. *Int J Mol Sci*. 2023;24(2):1.
51. Kasraei S, Azarsina M. Addition of silver nanoparticles reduces the wettability of methacrylate and silorane-based composites. *Braz Oral Res*. 2012;26(6):505–510. doi:10.1590/S1806-83242012000600004
52. Choi GH, Lee HJ, Lee SC. Titanium-adhesive polymer nanoparticles as a surface-releasing system of dual osteogenic growth factors. *Macromol Biosci*. 2014;14(4):496–507. doi:10.1002/mabi.201300368
53. Liu L, Cai R, Wang Y, et al. Preparation and characterization of AgNPs in situ synthesis on polyelectrolyte membrane coated Sericin/Agar film for antimicrobial applications. *Materials (Basel)*. 2018;11(7).
54. Ma Z, Mao Z, Gao C. Surface modification and property analysis of biomedical polymers used for tissue engineering. *Colloids Surf B Biointerfaces*. 2007;60(2):137–157. doi:10.1016/j.colsurfb.2007.06.019
55. Meng X, Zhang J, Chen J, et al. KR-12 coating of polyetheretherketone (PEEK) surface via polydopamine improves osteointegration and antibacterial activity in vivo. *J Mater Chem B*. 2020;8(44):10190–10204. doi:10.1039/D0TB01899F
56. Liu Y, Zheng Z, Zara JN, et al. The antimicrobial and osteoinductive properties of silver nanoparticle/poly (DL-lactic-co-glycolic acid)-coated stainless steel. *Biomaterials*. 2012;33(34):8745–8756. doi:10.1016/j.biomaterials.2012.08.010
57. Gao C, Peng S, Feng P, Shuai C. Bone biomaterials and interactions with stem cells. *Bone Res*. 2017;5:17059. doi:10.1038/boneres.2017.59
58. Kim BS, Kim JS, Park YM, Choi BY, Lee J. Mg ion implantation on SLA-treated titanium surface and its effects on the behavior of mesenchymal stem cell. *Mater Sci Eng C Mater Biol Appl*. 2013;33(3):1554–1560. doi:10.1016/j.msec.2012.12.061
59. Zhang K, Lin S, Feng Q, et al. Nanocomposite hydrogels stabilized by self-assembled multivalent bisphosphonate-magnesium nanoparticles mediate sustained release of magnesium ion and promote in-situ bone regeneration. *Acta Biomater*. 2017;64:389–400. doi:10.1016/j.actbio.2017.09.039
60. Shen T, Yang W, Shen X, et al. Polydopamine-assisted hydroxyapatite and lactoferrin multilayer on titanium for regulating bone balance and enhancing antibacterial property. *ACS Biomater Sci Eng*. 2018;4(9):3211–3223. doi:10.1021/acsbiomaterials.8b00791
61. Liu T, Wang Y, Zhong W, et al. Biomedical applications of layer-by-layer self-assembly for cell encapsulation: current status and future perspectives. *Adv Healthc Mater*. 2019;8(1):e1800939. doi:10.1002/adhm.201800939
62. Vasiliev G, Kubo AL, Vija H, et al. Synergistic antibacterial effect of copper and silver nanoparticles and their mechanism of action. *Sci Rep*. 2023;13(1):9202. doi:10.1038/s41598-023-36460-2
63. Ni Z, Wan M, Tang G, Sun L. Synthesis of CuO and PAA-regulated silver-carried CuO nanosheet composites and their antibacterial properties. *Polymers (Basel)*. 2022;14(24):5422. doi:10.3390/polym14245422
64. Mureed S, Naz S, Haider A, et al. Development of Multi-concentration Cu: Ag bimetallic nanoparticles as a promising bactericidal for antibiotic-resistant bacteria as evaluated with molecular docking study. *Nanoscale Res Lett*. 2021;16(1):91. doi:10.1186/s11671-021-03547-6